Phosphoproteomic Biomarkers Predicting Histologic Nonalcoholic Steatohepatitis and Fibrosis

ARTICLE *in* JOURNAL OF PROTEOME RESEARCH · MAY 2010

Impact Factor: 4.25 · DOI: 10.1021/pr100069e · Source: PubMed

10 AUTHORS, INCLUDING:

Ancha Baranova
George Mason University
213 PUBLICATIONS **3,276** CITATIONS
SEE PROFILE

Valerie S Calvert
George Mason University
53 PUBLICATIONS **2,758** CITATIONS
SEE PROFILE

Lance A Liotta
George Mason University
832 PUBLICATIONS **74,217** CITATIONS
SEE PROFILE

Emanuel Petricoin
George Mason University
363 PUBLICATIONS **22,303** CITATIONS
SEE PROFILE

research articles Journal of proteome research

Phosphoproteomic Biomarkers Predicting Histologic Nonalcoholic Steatohepatitis and Fibrosis

Zobair M. Younossi,*[,†,§] Ancha Baranova,[†,‡,§] Maria Stepanova,[†,§] Sandra Page,[‡] Valerie S. Calvert,[†,‡] Arian Afendy,[§] Zachary Goodman,[†,§] Vikas Chandhoke,[‡,§] Lance Liotta,[‡,§,||] and Emanuel Petricoin[‡,§,||]

Center for Liver Diseases, Inova Fairfax Hospital, 3300 Gallows Road, Falls Church, Virginia 22042, Center for the Study of Genomics in Liver Diseases, Molecular and Microbiology Department, George Mason University, Fairfax, Virginia 22030, Betty and Guy Beatty Center for Integrated Research, Inova Health System, 8110 Gatehouse Road, Falls Church, Virginia 22042, and Center for Applied Proteomics and Molecular Medicine, George Mason University, Manassas, Virginia 20110

Received January 26, 2010

The progression of nonalcoholic fatty liver disease (NAFLD) has been linked to deregulated exchange of the endocrine signaling between adipose and liver tissue. Proteomic assays for the phosphorylation events that characterize the activated or deactivated state of the kinase-driven signaling cascades in visceral adipose tissue (VAT) could shed light on the pathogenesis of nonalcoholic steatohepatitis (NASH) and related fibrosis. Reverse-phase protein microarrays (RPMA) were used to develop biomarkers for NASH and fibrosis using VAT collected from 167 NAFLD patients (training cohort, $N = 117$; testing cohort, $N = 50$). Three types of models were developed for NASH and advanced fibrosis: clinical models, proteomics models, and combination models. NASH was predicted by a model that included measurements of two components of the insulin signaling pathway: AKT kinase and insulin receptor substrate 1 (IRS1). The models for fibrosis were less reliable when predictions were based on phosphoproteomic, clinical, or the combination data. The best performing model relied on levels of the phosphorylation of GSK3 as well as on two subunits of cyclic AMP regulated protein kinase A (PKA). Phosphoproteomics technology could potentially be used to provide pathogenic information about NASH and NASH-related fibrosis. This information can lead to a clinically relevant diagnostic/prognostic biomarker for NASH.

Keywords: Nonalcoholic fatty liver disease (NAFLD) • nonalcoholic steatohepatitis (NASH) • fibrosis • reverse-phase protein microarrays (RPMA) • biomarker

Introduction

Nonalcoholic fatty liver disease (NAFLD) is the hepatic manifestation of metabolic syndrome[1,2] and is linked to insulin resistance, type II diabetes, and obesity.[2−5] In the U.S., NAFLD affects an estimated one-third of the population including children and adults, men and women, and a variety of ethnic groups.[6,7] NAFLD is diagnosed in patients whose fatty liver disease is unrelated to alcohol consumption, medication, or other causes of secondary fatty liver disease.[8] NAFLD encompasses a range of pathologies including steatosis alone (simple steatosis, SS), steatosis with nonspecific inflammation (SS-NSI), and nonalcoholic steatohepatitis (NASH) that might be complicated with hepatic fibrosis, NASH-related cirrhosis, and/or hepatocellular carcinoma.[9,10] Distinguishing NASH from SS is important because NASH can progress to more severe forms of liver disease, including cirrhosis and hepatocellular carcinoma, whereas SS remains benign in most patients.[9,11] Currently, liver biopsy is the only definitive way to diagnose and stage NAFLD, particularly for differentiating SS from NASH.[12] However, liver biopsy is an invasive procedure with inherent risks and is susceptible to sampling error.[13] Other methods such as ultrasonography and magnetic resonance are useful for detecting steatosis, but these methods are insensitive to steatosis less than 30% and cannot be used to distinguish NASH or fibrosis from simple steatosis.[14,15]

The pathogenesis of NASH and the molecular pathways distinguishing NASH from SS are not well understood. The progression of NAFLD has been linked to deregulated exchange of the endocrine signaling between adipose and liver tissue.[16] Because long-range cell signaling depends on the proteins, not mRNAs, protein profiling seems the most relevant high-throughput methods of discovering the deranged pathways contributing to the progression of NASH to cirrhosis which occurs in approximately 15−20% of the patients with NASH. On the other hand, most patients with SS do not progress to

* Corresponding author. Phone: (703) 776-2540. Fax: (703) 776-4388. E-mail: zobair.younossi@inova.org.
† Inova Fairfax Hospital.
‡ Molecular and Microbiology Department, George Mason University.
§ Inova Health System.
|| Center for Applied Proteomics and Molecular Medicine, George Mason University.

10.1021/pr100069e

Published on Web 05/04/2010

Table 1. Twenty-Seven Phosphoproteomics End Points Profiled in 167 Patients with NAFLD

antibody	phosphorylation end point	protein
pAMPKA1	S485	AMP-activate kinase, alpha 1 subunit
pAMPKB1	S108	AMP-activated protein kinase beta 1 subunit (noncatalytic)
pIRS1	S612	insulin receptor substrate 1
p4EBP1	S65	eIF4E-binding protein 1 (regulated by insulin)
peIF4G	S1108	translation initiation factor 4 gamma
pcAbl	T735	proto-oncogene tyrosine-protein kinase ABL1
peNOS/NOSIII	S116	nitric oxide synthase 3 (endothelial cell)
pFAK	Y397	focal adhesion kinase 1
pGSK3ab	Y279 Y216	glycogen synthase kinase-3 alpha/beta
pGSK3ab	S21 S9	glycogen synthase kinase-3 alpha/beta
pFKHR	S256	forkhead box O1
pFKHR-RL1	T24/32	forkhead box O1
pShc	Y317	SHC-transforming protein
pBAD	S136	Bcl2 antagonist of cell death
pBAD	S112	Bcl2 antagonist of cell death
pBAD	S155	Bcl2 antagonist of cell death
pmTOR	S2448	Serine/threonine-protein kinase mTOR
pp70S6	S371	ribosomal protein S6 kinase, 70 kDa
pp70S6	T389	ribosomal protein S6 kinase, 70 kDa
pp90RSK	S380	ribosomal protein S6 kinase, 90 kDa
pAKT	S473	RAC-alpha serine/threonine-protein kinase
pAKT	T308	RAC-alpha serine/threonine-protein kinase
pCREB	S133	cyclic AMP-responsive element-binding protein 1
pPKA C	T197	protein kinase C, alpha
pPKCaBII	T638/641	protein kinase C, beta (catalytic)
pPKCd	T505	protein kinase C, delta
pPKCtheta	T538	protein kinase C, theta

NASH or cirrhosis. Proteomic assays designed to evaluate the phosphorylation events that characterize the activated or deactivated state of the signaling cascades are especially useful for assessing kinase-driven signaling networks. Because reverse-phase protein microarray (RPMA) captures proteins in their phosphorylated or dephosphorylated forms, it suits the purpose of evaluating the state of the signaling networks in the adipose tissue related to NAFLD.[17] The proof of principle for this concept has been demonstrated earlier by an analysis of 54 different kinase substrates and cell signaling end points showing that an insulin signaling pathway is deranged in adipose tissue of NAFLD patients.[18] However, it remains to be seen whether these changes in the phosphoproteome end points have diagnostic significance. This study uses RPMA to develop a panel of biomarkers for NASH and fibrosis.

Materials and Methods

Patient Population and Pathology Assessments. Liver biopsy samples, visceral adipose tissue, blood samples, clinical data, and demographic data were collected from 167 patients at Inova Fairfax Hospital after informed consent. Visceral adipose (VAT) samples were collected from the omental fat located in the upper abdominal area above L4−L5 and immediately snap-frozen in liquid nitrogen. Liver specimens were fixed in formalin, routinely processed for histology, sectioned, and stained with hematoxylin−eosin and Masson trichrome. The Institutional Review Board of Inova Fairfax Hospital reviewed and approved this study.

The liver biopsy specimens were read by a single experienced hepatopathologist (ZG) who was blinded to all clinical and laboratory data. The slides were reviewed according to a predetermined histologic grading system. Hematoxylin and eosin stained slides were used to determine the extent of steatosis. The degree of steatosis was assessed in hematoxylin−eosin-stained sections and graded as an estimate of the percentage of tissue occupied by fat vacuoles as follows: 0 = none; 1 = <5%; 2 = 6−33%; 3 = 34−66%; 4 = >66%. Other histological features evaluated in hematoxylin−eosin sections included portal inflammation, lymphoplasmacytic lobular inflammation, polymorphonuclear lobular inflammation, Kupffer cell hypertrophy, apoptotic bodies, focal parenchymal necrosis, glycogen nuclei, hepatocellular ballooning, and Mallory−Denk bodies.

Fibrosis was assessed with the Masson trichrome stain. Portal fibrosis and interlobular pericellular fibrosis were graded as follows: 0 = none; 1 = mild; 2 = moderate; and 3 = marked. When present, bridging fibrosis was noted as few or many bridges, and cirrhosis was identified by parenchymal nodules surrounded by fibrous tissue. Cirrhosis was further categorized as incomplete or established, depending on the degree of loss of acinar architecture. Fibrosis was categorized into two groups: (1) none to minimal fibrosis and (2) advanced fibrosis. The "none to minimal fibrosis" group had no or only mild portal or pericellular fibrosis. The "advanced fibrosis" group had at least moderate portal or pericellular fibrosis, bridging fibrosis, or cirrhosis. Patients who had NASH or hepatic steatosis (with or without nonspecific inflammation) were considered to have NAFLD. NASH was defined as steatosis, lobular inflammation, and ballooning degeneration with or without Mallory−Denk bodies and/or fibrosis.[19]

It is important to note that training ($N = 117$) and test ($N = 50$) sets of samples were collected independently. Test samples were collected and processed for subsequent proteomics analysis after completion of the analysis of the training set. No matching of the training and test sample sets was performed; both training and test sample sets were derived from the cohort of morbidly obese patients who were undergoing bariatric surgery in our institution.

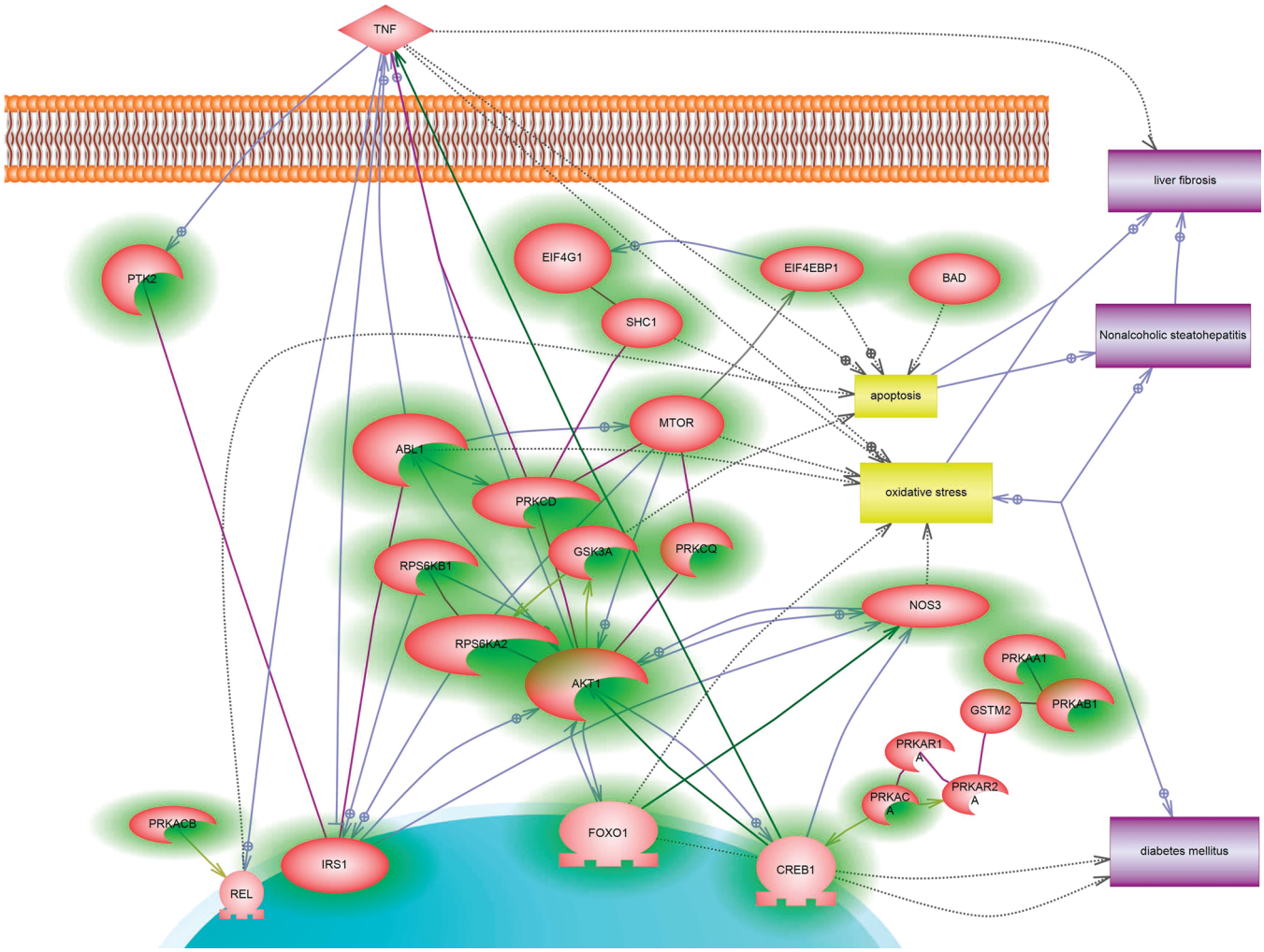

Figure 1. Model of the signaling cascades covered by 27 antibodies used for the phosphoproteomics events profiling in adipose samples of NAFLD patients.

Adipose Tissue Processing and Protein Extraction. An amount of 200 mg of each adipose tissue sample was transferred to a Pulse tube (Sumitomo Cryogenics of America Inc., Allentown, PA) along with 1.2 mL of lysis buffer containing a 1:1 mixture of 2X Tris-Glycine SDS Sample Buffer (Invitrogen Life Technologies, Carlsbad, CA) and Tissue Protein Extraction Reagent (Pierce, Rockford, IL) plus 2.5% β-mercaptoethanol and subjected to five rapid pressure cycles in the Barocycler NEP3299 (Pressure BioSciences, West Bridgewater, MA). Each cycle consisted of 20 s at 35 000 psi followed by 20 s at ambient pressure.

Reverse-Phase Protein Microarrays. The protein lysates were loaded into 384-well plates and each serially diluted in Lysis buffer to a 5-point dilution curve (neat, 1/2, 1/4, 1/8, and 1/16). Each dilution series was printed in duplicate onto nitrocellulose-coated glass slides (Whatman, Inc., Sanford, ME) with a 2470 Arrayer (Aushon BioSystems, Burlington, MA), outfitted with 350 μm pins, for a final deposited volume of approximately 33 nL per spot. The total protein in each spot ranged from 250 ng to 4 μg. Slides were desiccated and stored at −20 °C. Total protein was quantified in selected arrays that were stained with Sypro Ruby Protein Blot Stain (Molecular Probes, Eugene, OR) according to the manufacturer's instructions and visualized on an Affymetrix 428 Array Scanner (Santa Clara, CA). Before antibody staining, the lysate arrays were treated with mild Reblot antibody stripping solution (Chemicon, Temecula, CA) for 15 min at room temperature, washed 2 × 5 min in phosphate-buffered saline, and then incubated for at least 5 h in blocking solution [1 g I-block (Tropix, Bedford, MA), 0.1% Tween-20 in 500 mL of phosphate-buffered saline] at room temperature with constant rocking.

Protein Microarray Staining. Blocked arrays were stained with antibodies on an automated slide stainer (Dako Cytomation, Carpinteria, CA) using the Catalyzed Signal Amplification System kit according to the manufacturer's recommendation (CSA; Dako Cytomation). Briefly, endogenous biotin was blocked for 10 min with the biotin blocking kit (Dako Cytomation), followed by application of protein block for 5 min; primary antibodies were diluted in antibody diluent and incubated on slides for 30 min, and biotinylated secondary antibodies were incubated for 15 min. Signal amplification involved incubation with a streptavidin−biotin−peroxidase complex provided in the CSA kit for 15 min and amplification reagents (biotinyl−tyramide/hydrogen peroxide, streptavidin−peroxidase) for 15 min each. Development was completed by using diaminobenzadine/hydrogen peroxide as the chromogen/substrate. Slides were allowed to air-dry after development.

We specifically chose 27 primary antibodies (Table 1) associated with the signaling cascades that showed the largest variations in the measurements of the phosphoproteome

Table 2. Clinical Data for Patients with or Without NASH and with or without Severe (Stage 2+) Fibrosis (Training Cohort)[a]

parameter	no NASH	NASH	minimal or no fibrosis	advanced fibrosis
sample size, *N*	99	18	96	21
age, yrs	43.80 ± 10.76	43.11 ± 11.70	43.91 ± 10.76	42.71 ± 11.54
gender (% female) (*)(#)	82	39	79	57
race (% Caucasians)	73	89	76	71
BMI	47.08 ± 8.96	48.11 ± 8.74	47.34 ± 8.92	46.81 ± 8.97
waist, cm	134.48 ± 16.66	136.97 ± 16.65	134.44 ± 16.36	136.57 ± 17.95
type 2 diabetes (%)	22	35	23	29
hyperlipidemia (%)	41	38	44	25
hypertension (%)	53	71	52	71
smoking (%)	09	22	09	19
AST (*)(#)	22.14 ± 11.03	41.53 ± 32.29	22.05 ± 9.63	39.00 ± 32.75
ALT (*)	28.49 ± 16.25	53.41 ± 32.12	29.62 ± 16.95	44.50 ± 32.85
serum albumin mg/dl (*)	3.96 ± 0.49	4.25 ± 0.17	3.97 ± 0.49	4.12 ± 0.32
total bilirubin mg/dl (*)(#)	0.45 ± 0.21	0.61 ± 0.27	0.45 ± 0.21	0.58 ± 0.27
fasting serum glucose mg/dl	105.31 ± 38.13	128.85 ± 46.49	107.32 ± 39.43	118.25 ± 44.63
fasting total cholesterol mg/dl	197.86 ± 44.42	200.00 ± 31.36	198.49 ± 44.75	196.89 ± 31.89
fasting serum triglycerides mg/dl (*)	175.03 ± 177.29	231.69 ± 110.75	188.78 ± 185.29	164.84 ± 68.07

[a] Parameters significantly different between the cohorts with NASH and without NASH are denoted by (*). Parameters significantly different between the cohorts with moderate or severe fibrosis and with mild or no fibrosis are denoted by (#).

components in adipose tissue lysates of morbidly obese patients with and without NAFLD.[18] The RPMA, like all immunological techniques, rely on specific and well-performing antibodies. To that end, prior to use, each lot of each of these antibodies undergoes extensive prevalidation in our laboratory for (a) a single band on Western blot at the appropriate MW and (b) the appropriate ligand induction for phospho-specific antibodies (e.g., A431 ± EGF). Figure 1 shows the signaling pathways involving these antibodies. This diagram was built with Pathway Studio software (Ariadne Genomics). Secondary antibodies and dilutions included: biotinylated goat antirabbit IgG (H + L) 1:5000 (Vector Laboratories, Burlingame, CA) and biotinylated rabbit antimouse IgG 1:10 (Dako Cytomation).

Image Analysis. Stained slides were scanned individually on a UMAX PowerLook III scanner (UMAX, Dallas, TX) at 600 dpi and saved as TIF files in Photoshop 6.0 (Adobe, San Jose, CA). The TIF images for antibody-stained slides and Sypro-stained slide images were analyzed with MicroVigene image analysis software, version 2.200 (Vigenetech, North Billerica, MA), and Microsoft Excel 2000 software. Images were imported into Microvigene suit for spot finding, local background subtraction, replicate averaging, and total protein normalization, producing a single value for each sample at each end point.

Statistical Procedures. Regression models for predicting NASH and fibrosis (with these parameters used as dependent variables) were generated by stepwise bidirectional selection using data from the training cohort. The stability of the variable selection process and model design was verified at each step in a series of 10-fold cross-validation (10-CV) experiments. In those experiments, the complete cohort was partitioned into 10 subsamples. Of the 10 subsamples, a single subsample was retained as the validation data for testing the model, while the remaining 9 subsamples were used as training data; that process was repeated 10 times, with each of the 10 subsamples used exactly once as the validation data. The predictive power of the developed models, namely, the sensitivity, specificity, positive/negative predictive values, and area under the ROC-curve (AUC) with 95% confidence intervals (CIs), was also measured for each resulting model after completion of the 10-CV procedure. The regression analyses were executed with SAS 9.2 (Cary, NC), and the predictive performance of the models was collected with the MedCalc (Mariakerke, Belgium) statistical tool. Three types of the models were calculated using: (1) only the training cohort validated by the 10-CV method; (2) only the training cohort validated using the blinded test cohort; and (3) a combination of the training and test cohorts. *P* values ≤0.05 were considered significant.

Results

Clinical data for the training cohort ($N = 117$) are provided in Table 2. Three types of the models were developed, separately for NASH and advanced fibrosis: (1) clinical model only, which was based on clinical and demographic variables only; (2) proteomics model only, which was based on phosphoproteome profiles only; (3) combination model, which was based on a combination of clinical and phosphoproteomic parameters.

Models Predicting NASH. For NASH, the model based on a combination of clinical and phosphoproteomic parameters performed the best, with an AUC = 0.860 (0.780−0.919), sensitivity of 81.3%, and specificity of 87.0% (Table 3). This model included the following parameters: age, race, gender, diabetes status, AST, pAKT S473, and pIRS1 S612.

The remaining models predicting NASH (i.e., those based on clinical parameters only or proteomic data only) demonstrated marginally lower AUC values (0.837 and 0.771, respectively) but had substantially lower specificity (70.7% and 70.0%, respectively) and, therefore, unacceptably low positive predictive values (34.1% and 30.2%, respectively). Interestingly, negative predictive values (NPV) were well over 90% for all models.

Validation of the Models Predicting NASH. Validation of the models was based on the blinded test cohort ($N = 50$), which was not significantly different by any of the variables listed in Table 1 from the training cohort.

The histological description of the liver biopsy as well as the clinical and the biochemical variables remained blinded until completion of the analysis. The performance of the model in the validation was characterized by an AUC of 0.675 (95% CI, 0.518−0.809). Lowering of the validated AUC was due to the decrease of the positive predictive value that was 31.2 for the test cohort as compared to 52 for the training cohort, while the negative predictive value of the model was confirmed in the validation experiment (96.4%).

Table 3. Results for Modeling Efforts to Predict NASH Using Training Cohort ($N = 117$)[a]

parameters	*p*-value	sensitivity, % (95% CI)	specificity, % (95% CI)	PPV, % (95% CI)	NPV, % (95% CI)	significant parameters of the model
clinical only	<8.86 e^{-08}	87.5 (61.6−98.1)	70.8 (60.2−79.7)	34.1 (20.1−50.6)	97 (89.6−99.6)	race + gender + AST + Diabetes
proteomics only	<0.0003	72.2 (46.5−90.2)	69.7 (59.6−78.5)	30.2 (17.2−46.1)	93.2 (84.9−97.7)	peIF4G.S1108 + pGSK3aB.S21.9 + pIRS1.S612 + pPKCtheta.T538 + pShc.Y317
clinical + proteomics	<1.74 e^{-08}	81.3 (54.3−95.7)	87.0 (78.3−93.1)	52.0 (31.3−72.2)	96.4 (89.8−99.2)	age + race + gender + diabetes + AST + pAKT.S473 + pIRS1.S612

[a] PPV, positive predictive value; NPV, negative predictive value; CI, confidence interval.

Table 4. Results for Modeling Efforts to Predict Severe (Stage 2+) Fibrosis Using the Training Cohort ($N = 117$)[a]

parameters	*p*-value	sensitivity, % (95% CI)	specificity, % (95% CI)	PPV, % (95% CI)	NPV, % (95% CI)	significant parameters of the model
clinical only	<4.78e^{-06}	73.7 (48.8−90.8)	75.6 (64.9−84.4)	41.2 (24.7−59.3)	92.5 83.4−97.5	Age + diabetes + hyperlipidemia + hypertension + AST + platelets
proteomics only	<0.0003	81.0 (58.1−94.4)	76.0 (66.2−84.2)	42.5 (27.1−59.1)	94.8 87.2−98.5	pAMPKB1.S108 + pBAD.S112 + peIF4G.S1108 + pGSK3aB.S21.9 + pp70S6.T389 + pPKCaBII.T638.641 + PKCtheta.T538
clinical + proteomics	<1.95e^{-07}	79.0 (54.4−93.8)	73.17 (62.2−82.4)	40.5 (24.8−57.9)	93.7 84.7−98.2	age + diabetes + hyperlipidemia + hypertension + AST + platelets + pGSK3aB.S21.9 + pPKA.C.T197 + pPKCaBII.T638.641

[a] PPV, positive predictive value; NPV, negative predictive value; CI, confidence interval.

The performance of this model was assessed further by extending the training data set to all 167 patients by including the subjects whose clinical data were uncovered after the completion of the validation phase. This extension resulted in a model with an increase of the optimal threshold from 0.1593 to 0.2338, an AUC of 0.803 (CI 95% 0.731 to 0.863, $p < 2.47e^{-8}$), a sensitivity of 77.27%, and a specificity of 73.08%. The negative predictive value (NPV) of the retrained model was 95%.

Models Predicting Advanced Fibrosis. Overall, models predicting advanced fibrosis (stage ≥ 2) were less robust than those predicting NASH. Similar to the models predicting NASH, a combination of clinical and phosphoproteomic parameters delivered better performance than any other model based on clinical or phosphoproteomic variables alone.

The resulting fibrosis predicting model had an AUC of just 0.807, 78.9% sensitivity, and 73.2% specificity. This model included the following parameters: age, type 2 diabetes, hyperlipidemia, hypertension, AST, platelets, pGSK3aB Y279/216, pPKAC T197, and pPKA C T197/641 (Table 4).

Unlike models predicting NASH, predictions of fibrosis using clinical parameters only or proteomic data only lead to the proportional changes in both sensitivity (73.7% and 81.0%, respectively) and specificity values (75.6% and 76.0%, respectively). However, positive predictive values of generated models remained low in all three fibrosis panels (Table 3), while negative predictive values (NPV) remained over 90%.

Validation of the Models Predicting Advanced Fibrosis. Validation of the fibrosis predicting models was performed using the same approach; the best performance of the fibrosis model was determined by extending the validation cohort to all patients. In this case, the optimal threshold was increased from 0.0024 to 0.0511, an AUC of 0.745 (CI 95%: 0.666 to 0.813, $p < 0.0001$), a sensitivity of 66.67%, and a specificity of 74.59%. The negative predictive value (NPV) of the retrained model was 91.9%.

Discussion

This study investigated biomarker profiles for predicting NASH or significant fibrosis in a cohort of patients with biopsy-proven NAFLD. We used several common clinical variables as well as parameters that measure the deregulation of the protein phosphorylation events that reflect the state of cell signaling within the adipose tissue. To this end, we employed reverse-phase protein microarray (RPMA) assays that individually measure proteins in their inactivated and activated/phosphorylated forms, providing a unique window into the functional activity of the signaling networks in human adipose tissue. We specifically chose to analyze 27 specific signaling proteins contained within cascades that were previously shown to have the largest variation in adipose tissue lysates of morbidly obese patients,[18] particularly insulin signaling and cell death branches of the GSK3/mTOR/PKC regulated network (Figure 1).

In this NAFLD cohort, NASH was accurately predicted by a model that included measurements of the two components of the insulin signaling pathway, AKT kinase and Insulin receptor substrate 1 (IRS1). Activated AKT kinases normally suppress Glycogen Synthase Kinase-3 (GSK-3) and, thus, exhibit an antidiabetic effect[20,21] primarily through insulin sensitization in peripheral tissues. Suppression of GSK-3 precludes phosphorylation of IRS1 and, therefore, prevents an impairment of insulin-stimulated glucose uptake, GLUT4 translocation, and glycogen synthesis mediated by the IRS-1/PI-3K/Akt/GSK-3 pathway. As NASH is tightly linked to insulin resistance[3] and tends to progress more rapidly in diabetics,[22] the ability of a concerted change in the activity of AKT and IRS1 to predict the presence of this disorder is expected.

The models predicting advanced fibrosis were less reliable when predictions were based on phosphoproteomic data, clinical data, or a combination of both. The best performing model relied on levels of the phosphorylation of GSK3 as well

as on two subunits of cyclic AMP regulated protein kinase A (PKA). In hepatocytes, simulating PKA increases the production of procollagen-alpha;[23] in adipocyte, PKA plays a key role in the regulation of important metabolic processes, i.e., lipolysis and thermogenesis.[24] Recent work shows that in adipocytes the stimulation of PKA facilitates the release of lL-6,[25] a known contributor to fibrotic changes in NAFLD patients.[26] Therefore, links between activation of the PKA-GSK3 axis in adipose and liver fibrosis shall be studied in greater detail in future studies. It is also important to note that several components of metabolic syndrome (diabetes, hyperlipidemia, and hypertension) were included in the model predicting advanced fibrosis. These findings confirm previous work showing that NAFLD patients with metabolic conditions, especially type 2 diabetes, are at risk for significant hepatic fibrosis.

The initial validation strategy confirmed that our models were more valuable for "ruling out" the potentially progressive forms of NAFLD (NASH or advanced fibrosis) than for "ruling in", as reflected by high NPV and low PPV values. Interestingly, previously described NASH diagnosing models built upon the noninvasive measurements of necrosis and apoptosis[27−29] had similarly low PPV values. It is plausible that within the multihit pathogenic hypothesis of NASH, which involves insulin resistance, oxidative stress, apoptosis, and adipokine-cytokine disturbance, these hits may come as a collection of aggregate "microhits". In fact, these microhits may come in any order, as each of them contributes to the damage caused by other inciting factors. If biomarker panels seek to detect the presence or absence of microhits rather than the quantity or sequence of microhits, the associated damage, low cutoff values chosen for the validation of the model, will translate as a combination of low PPV values (progressive disease is "ruled-in" as the "microhit in question" was detected) with high NPV values (progressive disease is "ruled-out" as no "microhit in question" is detected). To overcome the intrinsic limitation of this type of predictive model, the diagnostic panel should include biomarkers that thoroughly cover all aspects of the pathogenesis of NASH. Nevertheless, these types of biomarker panels revealed low PPVs. We anticipate that NASH patients with a false positive diagnosis would not be harmed and might benefit from clinical management, which relies primarily on exercise and weight loss. Another way to improve performance of the existing model is to adjust its threshold after testing additional subjects. Further extension of the training data set and subsequent independent validation experiments are under way.

In conclusion, characterization of phosphoproteome changes in adipose and other tissues could eventually lead to the development of targeted therapies for NAFLD.[17] This is especially important because kinases are targets of many pharmaceutical drugs.[30] Because the phosphorylation status of proteins is reversible, recently developed technologies can detect the phosphorylated state of a protein at the time of sampling. This capability is made possible by the advent of antibodies designed to target proteins in their phosphorylated or dephosphorylated form. These results suggest that phosphoprotein biomarkers could potentially be used in a clinical setting to identify patients with NASH. Furthermore, the results shed light on the biological or pathogenic pathways that may be involved in the pathogenesis of NASH.

Statement of Clinical Relevance

NAFLD and NASH are among the most common causes of liver disease in the U.S. Currently, diagnosis of NASH requires a liver biopsy which is invasive and costly. New biomarkers based on proteomics technology could provide information that could potentially lead to the development of noninvasive tests for NASH. This study reports the use of reverse-phase protein microarrays (RPMA) for patients with histologically proven NASH and NASH-related fibrosis. The study provides evidence that RPMA not only can be used for studying NASH but also could represent an excellent technology for development of diagnostic or prognostic biomarkers for this important liver disease.

Abbreviations. NAFLD, nonalcoholic fatty liver disease; NASH, nonalcoholic steatohepatitis; SS, simple steatosis; SSNSI, steatosis with nonspecific inflammation; RPMA, reverse-phase protein microarrays; VAT, visceral adipose tissue; AUC, area under the curve; NPV, negative predictive values; PPV, positive predictive values; AST, aspartate aminotransferase; AKT, RAC-alpha serine/threonine-protein kinase; GLUT4, glucose transporter type 4; GSK-3, glycogen synthase kinase-3; IRS1, insulin receptor substrate 1; mTOR, mammalian target of rapamycin; PI-3K, phosphoinsositide kinase-3; PKC, protein kinase C.

References

(1) Marchesini, G.; Brizi, M.; Bianchi, G.; Tomassetti, S.; Bugianesi, E.; Lenzi, M.; et al. Nonalcoholic fatty liver disease: a feature of the metabolic syndrome. *Diabetes* **2001**, *50*, 1844–1850.

(2) Sanyal, A. J.; Campbell-Sargent, C.; Mirshahi, F.; Rizzo, W. B.; Contos, M. J.; Sterling, R. K.; et al. Nonalcoholic steatohepatitis: association of insulin resistance and mitochondrial abnormalities. *Gastroenterology* **2001**, *120*, 1183–1192.

(3) Choudhury, J.; Sanyal, A. J. Insulin resistance in NASH. *Front. Biosci.* **2005**, *10*, 1520–1533.

(4) Li, Z.; Clark, J.; Diehl, A. M. The liver in obesity and type 2 diabetes mellitus. *Clin. Liver Dis.* **2002**, *6*, 867–877.

(5) Chitturi, S.; Abeygunasekera, S.; Farrell, G. C.; Holmes-Walker, J.; Hui, J. M.; et al. NASH and insulin resistance: Insulin hypersecretion and specific association with the insulin resistance syndrome. *Hepatology* **2002**, *35*, 373–379.

(6) Browning, J. D.; Szczepaniak, L. S.; Dobbins, R; Nuremberg, P; Horton, J. D.; Cohen, J. C.; Grundy, S. M.; Hobbs, H. H. Prevalence of hepatic steatosis in an urban population in the United States: impact of ethnicity. *Hepatology* **2004**, *40*, 1387–1395.

(7) Lavine, J. E.; Schwimmer, J. B. Nonalcoholic fatty liver disease in the pediatric population. *Clin. Liver Dis.* **2004**, *8*, 549–558.

(8) Neuschwander-Tetri, B. A. Nonalcoholic steatohepatitis and the metabolic syndrome. *Am. J. Med. Sci.* **2005**, *330*, 326–335.

(9) Younossi, Z. M.; Diehl, A. M.; Ong, J. P. Nonalcoholic fatty liver disease: an agenda for clinical research. *Hepatology* **2002**, *35*, 746–752.

(10) Baranova, A.; Younossi, Z. M. Adipokines in nonalcoholic fatty liver disease. In *Nutrition and Health: Adipose Tissue and Adipokines in Health and Disease*; Fantuzzi, G., Mazzone, T., Eds.; Humana Press Inc.: Totowa, NJ, 2006.

(11) Matteoni, C. A.; Younossi, Z. M.; Gramlich, T.; Boparai, N.; Liu, Y. C.; McCullough, A. J. Nonalcoholic fatty liver disease: a spectrum of clinical and pathological severity. *Gastroenterology* **1999**, *116*, 1413−1419.

(12) Duvnjak, M.; Lerotić, I.; Barsí, N.; Tomasić, V.; Virović Jukić, L.; Velagić, V. Pathogenesis and management issues for non-alcoholic fatty liver disease. *World J. Gastroenterol.* **2007**, *13*, 4539–4550.

(13) Ratziu, V.; Charlotte, F.; Heurtier, A.; Gombert, S.; Giral, P.; Bruckert, E.; et al. Sampling variability of liver biopsy in nonalcoholic fatty liver disease. *Gastroenterology* **2005**, *128*, 1898–1906.

(14) Collantes, R.; Ong, J. P.; Younossi, Z. M. Nonalcoholic fatty liver disease and the epidemic of obesity. *Clev. Clin. J. Med.* **2004**, *71*, 657–664.

(15) Tobari, M.; Hashimoto, E.; Yatsuji, S.; Torii, N.; Shiratori, K. Imaging of nonalcoholic steatohepatitis: advantages and pitfalls of ultrasonography and computed tomography. *Intern. Med.* **2009**, *48*, 739–746.

(16) Delgado, J. S. Evolving trends in nonalcoholic fatty liver disease. *Eur. J. Intern. Med.* **2008**, *19*, 75–82.

(17) Espina, V.; Geho, D.; Mehta, A. I.; Petricoin, E. F., III; Liotta, L. A.; Rosenblatt, K. P. Pathology of the future: molecular profiling for targeted therapy. *Cancer Invest.* **2005**, *23*, 36–46.

(18) Calvert, V. S.; Collantes, R.; Elariny, H.; Afendy, A.; Baranova, A.; Mendoza, M.; et al. A systems biology approach to the pathogenesis of obesity-related nonalcoholic fatty liver disease using reverse phase protein microarrays for multiplexed cell signaling analysis. *Hepatology* **2007**, *46*, 166–172.
(19) Bondini, S.; Kleiner, D. E.; Goodman, Z. D.; Gramlich, T.; Younossi, Z. M. Pathologic assessment of non-alcoholic fatty liver disease. *Clin. Liver Dis.* **2007**, *11*, 17–23.
(20) Rayasam, G. V.; Tulasi, V. K.; Sodhi, R.; Davis, J. A.; Ray, A. Glycogen synthase kinase 3: more than a namesake. *Br. J. Pharmacol.* **2009**, *156*, 885–898.
(21) Wagman, A. S.; Johnson, K. W.; Bussiere, D. E. Discovery and development of GSK3 inhibitors for the treatment of type 2 diabetes. *Curr. Pharm. Des.* **2004**, *10*, 1105–1137.
(22) Rafiq, N.; Bai, C.; Fang, Y.; Srishord, M.; McCullough, A.; Gramlich, T.; Younossi, Z. M. Long-term follow-up of patients with nonalcoholic fatty liver. *Clin. Gastroenterol. Hepatol.* **2009**, *7*, 234–238.
(23) Che, J.; Chan, E. S.; Cronstein, B. N. Adenosine A2A receptor occupancy stimulates collagen expression by hepatic stellate cells via pathways involving protein kinase A, Src, and extracellular signal-regulated kinases 1/2 signaling cascade or p38 mitogen-activated protein kinase signaling pathway. *Mol. Pharmacol.* **2007**, *72*, 1626–1636.
(24) McKnight, G. S.; Cummings, D. E.; Amieux, P. S.; Sikorski, M. A.; Brandon, E. P.; Planas, J. V.; Motamed, K; Idzerda, R. L. Cyclic AMP, PKA, and the physiological regulation of adiposity. *Recent Prog. Horm. Res.* **1998**, *53*, 139–159.
(25) Antunes, T. T.; Gagnon, A.; Bell, A.; Sorisky, A. Thyroid-stimulating hormone stimulates interleukin-6 release from 3T3-L1 adipocytes through a cAMP-protein kinase A pathway. *Obes. Res.* **2005**, *13*, 2066–7201.
(26) Wieckowska, A.; Papouchado, B. G.; Li, Z.; Lopez, R.; Zein, N. N.; Feldstein, A. E. Increased hepatic and circulating interleukin-6 levels in human nonalcoholic steatohepatitis. *Am. J. Gastroenterol.* **2008**, *103*, 1372–1379.
(27) Baranova, A.; Younossi, Z. M. The future is around the corner: Noninvasive diagnosis of progressive nonalcoholic steatohepatitis. *Hepatology* **2008**, *47*, 373–375.
(28) Guha, I. N.; Parkes, J.; Roderick, P.; Chattopadhyay, D.; Cross, R.; Harris, S.; et al. Noninvasive markers of fibrosis in nonalcoholic fatty liver disease: Validating the European Liver Fibrosis Panel and exploring simple markers. *Hepatology* **2008**, *47*, 455–460.
(29) Younossi, Z. M.; Jarrar, M.; Nugent, C.; Randhawa, M.; Afendy, M.; Stepanova, M.; et al. A novel diagnostic biomarker panel for obesity-related nonalcoholic steatohepatitis (NASH). *Obes. Surg.* **2008**, *18*, 1430–1437.
(30) Cohen, P. Protein kinases--the major drug targets of the twenty-first century? *Nat. Rev. Drug Discovery* **2002**, *1*, 309–315.

PR100069E